Geometric modelling for virtual colon unfolding

Vilanova Bartroli, A.; Gröller, E.

Published in:
Geometric modeling for scientific visualization

Published: 01/01/2003

Citation for published version (APA):
Vilanova, A., & Gröller, E. (2003). Geometric modelling for virtual colon unfolding. In G. Brunnet (Ed.), Geometric modeling for scientific visualization. (pp. 453-468). (Mathematics and visualization). Berlin: Springer.

Geometric Modelling for Virtual Colon Unfolding

Anna Vilanova[1] and Eduard Gröller[2]

[1] Department of Biomedical Engineering
Eindhoven University of Technology
a.vilanova@tue.nl

[2] Institute of Computer Graphics and Algorithms
Vienna University of Technology
meister@cg.tuwien.ac.at

Summary. A virtual endoscopic view is not necessarily the best way to examine a hollow organ, such us, the colon. The inner surface of the colon is where polyps are located, and therefore what is examined by the physicians. A flight through the colon using a common endoscopic view shows a small percentage of the inner surface. Virtually unfolding of the colon can be a more efficient way to look at the inner surface. We propose two methods to unfold the colon: a method that unfolds the colon locally using local projections, and a method that obtains a global unfolding of the colon by achieving a suitable parameterization of its surface.

1 Introduction

Most of the virtual endoscopy applications presented in the last years concentrate on simulating the view of a real endoscope. This is the view that endoscopists are used to, and it is useful for certain applications, like in an intraoperative scenario. However, it is not necessarily the best way to inspect the inner surface of an organ. Actually, a real endoscope and organ are subject to physical limitations that a virtual endoscope and organ do not have. In this chapter, we concentrate on virtual colonoscopy, which focuses on the examination of the colon.

Physicians are mainly interested in visualizing the inner surface of the colon which is where polyps can be detected with endoscopy. It is important that the physician can estimate the size of polyps, since large polyps are more likely to develop into malignancies. The usual endoscopic view visualizes just a small part of the surface. Furthermore, it is difficult to detect polyps that are situated behind the folds of the colon. An efficient way to inspect the inner surface would be to open and unfold the colon, and then examine its internal surface. Unfortunately, this cannot be done in reality, if we want that the patient survives. On the other hand, there is no patient damage if this dissection of the organ can be achieved virtually with the medical data obtained by CT or MRI (i.e., the virtual organ). The resulting unfolded model has to facilitate the physician's inspection and detection of polyps.

In this chapter, we present different approaches to unfold the colon. After an overview of the existing methods, we present in detail two methods: a method that unfolds the colon locally using local projections, and a method that obtains a global unfolding of the colon.

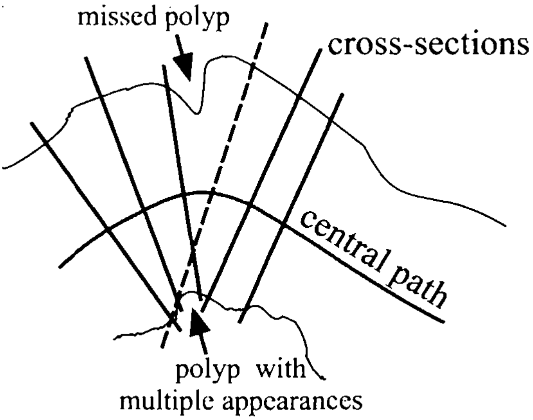

Fig. 1. Illustration of the possible undersampling and multiple appearance of polyps due to intersections of the cross-sections in high curvature areas. The dashed cross-section line produces a multiple appearance of the polyp.

2 Related Work

Wang et al. [20] proposed a technique to straighten and unravel an organ virtually. Their approach starts with defining a path which is placed as close to the center of the object as possible. Then, a sequence of frames is calculated. For each frame, a cross-section orthogonal to the path tangent is calculated. The central path is straightened and the cross-sections are piled to form a stack. As a last step, the straightened colon is unfolded by tracing rays in radial directions to the path. The result is a volumetric model of the unfolded colon. The model is displayed afterwards using standard volume rendering techniques. This method can be seen as a resampling and parameterization operation.

However, one of the main problems of this technique appears in high curvature areas of the central path, i.e., at path locations where the radius of curvature is bigger than the organ diameter. In such cases, orthogonal cross-sections intersect each other in some regions or are far apart in some other regions (see figure 1). As a consequence, a polyp can appear more than once in the unfolded model or it can be missed completely. These problems are the consequence of undersampling and an ambiguous parameterization of the organ surface.

In later works Wang et al. [18, 19] try to overcome these problems. The authors use electrical field lines generated by a locally charged path to govern curved cross-sections instead of planar sections. The cross-sections tend to diverge avoiding conflicts. If the complete path is charged then the curved cross-sections will not intersect. However, for each point of the field lines the contribution of each charge on the path must be calculated. This operation is computationally so expensive that the authors propose to just locally charge the path. A small segment of the path contains the charges for each cross-section. In this way, the method is feasible in practice, but it cannot ensure anymore that the curved cross-sections will not intersect each other. In other words, it cannot ensure that the parametrization of the space will be unambiguous. Furthermore, the undersampling is still a problem.

Other authors propose methods to flatten a polygonal representation of the colon surface. These techniques involve tasks that have already been used in texture-mapping for computer graphics. A major step thereby is to come up with a suitable surface parameterization. For texture mapping, this parameterization is used to assign texture values to surface points. For surface flattening the parameterization allows to display surface values (e.g., color) in the 2D parameter space [13]. Many techniques are dealing with texture distortions which generally cannot be avoided entirely. The distortions depend on the chosen surface-parameterization characteristics (e.g., length and area preserving [2], angle preserving [6] or a combination of both [3,9]).

Haker et al. [5] use conformal (i.e., angle preserving) texture mapping to map the polygonal colon surface to a plane. One of the main problems of this method is that a highly accurate segmentation is necessary to ensure good results for diagnosis. The entire polygonal surface is flattened. The result is a triangulated plane where the polyps have also been flattened. Shading is applied to the flattened surface using the normals of the original surface and the color-coded mean curvature. This is the only information which helps the physician in identifying polyps in the unfolded plane. Furthermore, the surface needs to be smoothed to achieve a good mean-curvature calculation which can imply smoothing and missing polyps.

In the previous methods, the whole colon surface was unfolded or flattened. To increase the visible surface, Paik et al. [12] propose to use different camera projections. With a normal endoscopic view just 8% of the solid angle of the camera is seen in each frame. Paik et al. project the whole solid angle of the camera by map projection techniques used for geographical charts. They suggest to use the Mercator projection for mapping the solid angle to the final image. This technique samples the solid angle of the camera, then the solid angle is mapped onto a cylinder which is mapped finally to the image. This method generates a video that the physician has to inspect.

Serlie et al. [14] present a method based on image-based rendering. In a pre-processing step, a cubic environment map is calculated at each camera position along the central path. These environment maps can be used to obtain real-time navigation using image-based rendering, as proposed by Wegenkittl et al. [21]. Serlie et al. [14] also propose to display these cubic maps unfolded in order that the physician has a 360 degrees field of view.

All these methods introduce some kind of deformation. Flattening a surface in 3D space onto a 2D plane introduces distortions unless the surface has zero Gaussian curvature. [11]

3 Local Colon Unfolding

In this section, we propose a method to unfold the colon using a new camera projection technique. This method [17] generates a video where each frame is a local unfolding of the organ. It allows to inspect locally unfolded regions such that multiple appearances of polyps do not occur. This method is similar to the one proposed by Serlie et al. [14].

The presented method involves moving a camera along the central path of the colon. Several techniques can be used to generate a smooth central path (see, e.g., Vilanova et al. [15]).

At each camera position along the central path, an orthogonal coordinate system is taken which specifies the location and orientation of a cylinder. One coordinate axis is given by the tangent vector of the central path. The other axes are in the plane orthogonal to the central path at the camera position. The Frenet frame is commonly used to define a coordinate system for a point on a curve. However, it is not a good choice in our case. Firstly, the Frenet frame is not defined in linear portions of the central path. Secondly, by moving along the path, the two vectors orthogonal to the tangent vector can rotate considerably, thus reducing coherence between adjacent frames. Instead of the Frenet frame, we use a rotation-minimizing coordinate frame as presented by Klok [8].

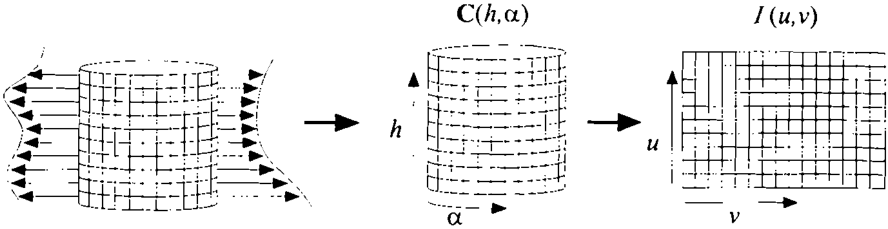

Fig. 2. Illustration of the projection procedure. A region of the organ surface is projected onto the cylinder $\mathbf{C}(h,\alpha)$. Then, the cylinder is mapped to the image $I(u,v)$.

For each camera position, a small cylinder $\mathbf{C}(h,\alpha)$[1] tangent to the path is defined. The point in the middle of the cylinder axis corresponds to the camera position. For each ray, direct volume rendering is used to calculate the color which corresponds to the cylinder point where the ray was projected. Finally, the colored cylinder with the sampled rays is developed into a 2D image $I(u,v)$ by a simple mapping function $\mathbf{f} : (h,\alpha) \rightarrow (u,v)$ (see figure 2). The simplest mapping function is the identity where $\mathbf{f}(h,\alpha) = (h,\alpha)$.

The cylinder axis must be short enough, such that the cylinder does not penetrate the surface of the colon. This can be done by taking into account the distance of the path to the organ surface.

The result is a video where each frame shows the projection of a small part of the inner surface of the organ onto a cylinder. If the camera is moved slowly enough the coherence between frames will be high and the observer will be able to follow the movement of the surface and polyps.

In high curvature areas, the intersection of cross-sections also occurs (see figure 1). However, crossing of rays can happen just between frames, which does not cause a multiple appearance of a polyp within a single image. Moving along the central path in a high curvature area, a polyp might move up and down (due to

[1] Throughout this chapter, scalars are given in italics and vectors in bold typeface. Angles are denoted by Greek letters. For example, $\mathbf{C}(h,\alpha)$ is a function which returns a vector (point) and has as parameters two scalars h and α, where α is an angle.

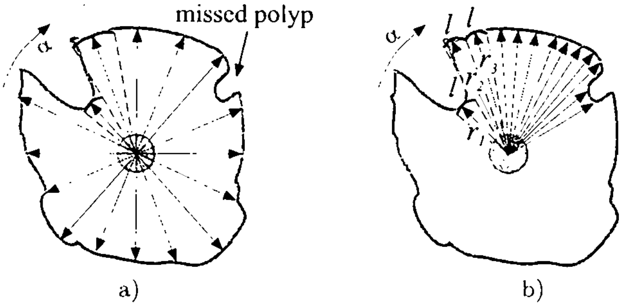

Fig. 3. **a)** Constant angle sampling: it is shown that different surface lengths are represented by the same length in the cylinder. **b)** Perimeter sampling: same length but different angle.

crossing rays), but it is clearly identified as a single object. The user is able of tracking the polyp movement if the coherence between frames is high enough.

The sampling distance (i.e., the distance between two consecutive rays) in the h-direction is constant, and it must be at most half of the size of a voxel (see figure 2). In this way, correct sampling (with respect to the Nyquist limit) is possible in the h-direction.

In the next sections, two methods are described which project the organ surface onto the cylinder depending on the sampling of angle α, i.e., constant angle sampling and perimeter sampling.

3.1 Constant Angle Sampling

Constant angle sampling means that the angle between consecutive rays in the α-direction is constant for rays with the same h-value. Figure 3a illustrates how this sampling is done. Using this method, the cylinder is sampled uniformly but not the organ surface.

The advantage of this method is that the relationship between both directions is preserved locally. Therefore, the angles are locally preserved too. An image generated by this method can be seen in figure 4a.

On the other hand, the area of the projected region is not preserved (see figure 3a). Therefore, the size of a projected polyp depends on the distance of the cylinder axis to the organ surface cavity. Consequently, the physician cannot trust the sizes of the projected polyps. With constant sampling, polyps can be missed if the angle increment is too large (see figure 3a). If the sampling distance is too small, rays are traced where it would not be necessary. This makes the method inefficient.

3.2 Perimeter Sampling

With perimeter sampling, rays are calculated such that the surface length that they represent is constant. A constant sample length l is defined. l must be at most half the size of a voxel to stay above the Nyquist frequency and therefore not to miss any important feature. l should have the same value as the sampling distance in the h-direction to preserve the ratio, or proportion, in the final mapping.

The algorithm incrementally calculates the ray directions which are in the plane defined by a certain value of h. The angle between the current ray and the next one is computed such that the length of the surface sample that the current ray represents is l in the α-direction (see figure 3b). r_i is defined as the distance from the cylinder axis to the surface point hit by the ith ray. The surface sample length in the α-direction that a ray represents is approximated by the arc with radius r_i. Therefore, the value of the angle increment for the next ray is estimated as $\frac{l}{r_i}$ radians. This projection method projects the organ surface to a generalized cylinder whose radii are not constant within the cylinder. Moving along the central path, varying perimeter lengths are represented by a varying number of rays. Therefore, the generalized cylinder is not mapped to a complete rectangular domain (see figure 4b). The mapping function $\mathbf{f}$ in this case maps each sampled ray to a pixel in the image (i.e., each pixel corresponds to an area of size $l \times l$ on the surface). The projected point that corresponds to the first ray is positioned on a vertical line in the center of the image. Then, from left to right, the ray values are mapped onto the image until the perimeter length is reached.

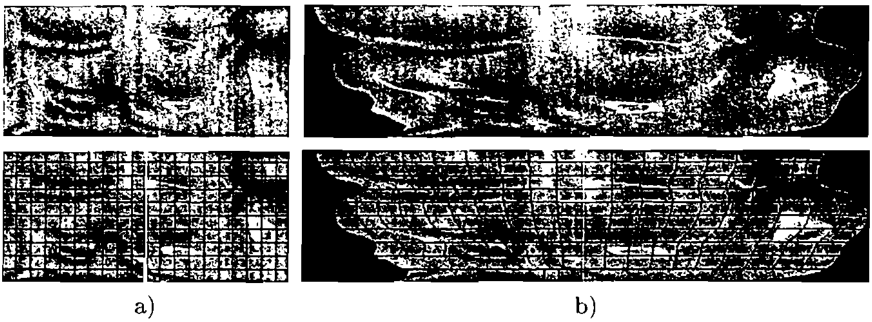

Fig. 4. a) Constant angle sampling of the organ surface. **b)** Same camera position as a) but with perimeter sampling. The bottom images show a grid with constant angle α.

This projection is area preserving. The relative sizes of surface elements are preserved in the image plane and do not depend on the distance of the cylinder axis to the surface. On the other hand, a distortion is introduced with respect to the h and α-directions, so the angles are not preserved anymore. At the vertical center line of the image, no distortion occurs, but the distortion increases progressively when we move to the left or right. Figure 4b shows an image generated with perimeter sampling. The superimposed grid corresponds to a regular grid in a constant angle sampling of the cylinder.

4 Nonlinear Colon Unfolding

The method presented in section 3 requires that the physician reviews a video and cannot visualize the complete surface at once. In this section, we describe a method [16] to obtain a complete model of the unfolded colon. This method uses similar ideas as the method by Wang et al. [20]. The technique provides solutions to multiple appearances of polyps, distortion and undersampling. In our approach, the colon unfolding does not produce a surface but a height field (distance of the colon surface to a central path). This avoids that the polyps are flattened as with the methods proposed by Haker et al. [5]. Furthermore, the height field gives a more natural visualization than a color-coded flattened surface.

Unfolding the colon can be divided into three main steps: nonlinear ray casting, which solves the problem of multiple appearances of polyps; nonlinear 2D scaling, which reduces the distortion due to nonuniform sampling; and resampling, which avoids to miss polyps.

As in local unfolding, a central path is calculated. A distance map is generated from the central path [10]. The distance map contains the distance to the nearest point on the central path. A coordinate frame is moved along the path. For each path position, rays are initialized in the plane orthogonal to the path, following radial directions (constant angle sampling). To avoid multiple appearances of polyps in high curvature areas of the path, the rays follow the negative gradient direction of the precalculated distance map. The rays are not straight lines anymore. They do not cross each other, but converge at most (see figure 5). Nonlinear ray casting has already been investigated before by several authors (e.g., Gröller [4]). Section 4.1 explains how these rays are traced.

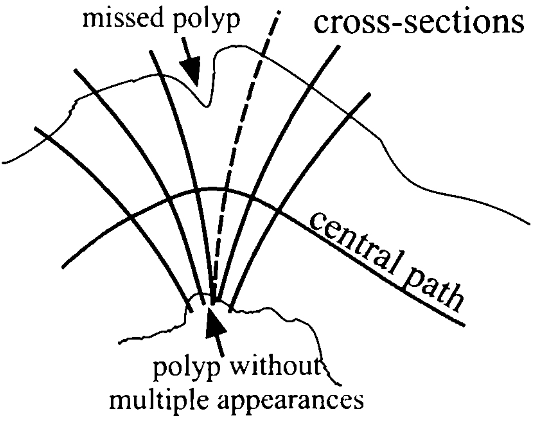

Fig. 5. Elimination of multiple polyp appearances by nonlinear ray casting.

Along each curved ray, direct volume rendering is performed. The ray is terminated when it hits the surface of the colon. The result of the nonlinear ray casting can be interpreted as a 2D cylindrical parameterization of the inner colon surface. One parameter corresponds to the position along the path. The second parameter specifies the ray within the plane orthogonal to the current path position. The distances between ray origins on the central path and intersected points on the colon surface determine a height field. The height field is unfolded, and the result corresponds to a parallel projection of the unfolded height field.

Nonlinear ray casting samples the height field nonuniformly. A straightforward unfolding to a regular grid (i.e., a uniform parameterization) contains severe area distortions and is therefore not optimal. In a second step, an iterative scaling transforms the previously generated 2D parameter grid in order to compensate for these distortions. After the scaling, the ratios between the area that the samples represent and their area in the 2D grid are approximately equal. The second step is based on nonlinear 2D scaling that is used in a similar way for magnification fields in information visualization [7]. In section 4.2, the algorithm is described in detail. Afterwards, the colon surface is resampled with an adequate minimum sampling rate using the transformed 2D grid.

4.1 Nonlinear Ray Casting

The central path of the colon is described by a parametric curve $\mathbf{c}(v)$. We define $dist(\mathbf{p}) : \mathbb{R}^3 \rightarrow \mathbb{R}$ as a function which gives the minimum distance between a point $\mathbf{p}$ and $\mathbf{c}(v)$. $dist(\mathbf{p})$ is sampled in a discrete distance map $Dist(\mathbf{q}) : \mathbb{N}^3 \rightarrow \mathbb{R}$ where $\mathbf{q}$ is a voxel position in the volume. A reconstruction filter is applied to $Dist(\mathbf{q})$ to approximate $dist(\mathbf{p})$(see Vilanova et al. [16] for details).

$dist(\mathbf{p})$ is continuous in the first derivative nearly everywhere. Exceptions are ridge and valley lines of the distance map $dist(\mathbf{p})$. $dist(\mathbf{p})$ induces a vectorfield that is defined by the gradient, $-\nabla dist(\mathbf{p})$. It is known that trajectories of such vectorfields will not cross each other and are unambiguous (see Abraham et al. [1] for details). These trajectories will correspond to our nonlinear rays. The nonlinear rays are traced from the central path in uphill direction, i.e., along the negative gradient direction $-\nabla dist(\mathbf{p})$. Furthermore, in our situation, trajectories will not produce cycles, since it is impossible to return to the same point by always moving uphill. In the worst case, the nonlinear rays will merge in ridge and valley lines, but they will not cross. With these curved rays the multiple appearance of polyps is avoided and an unambiguous and correct parameterization of the inner colon surface is obtained.

Casting of Nonlinear Rays

The first step to trace the nonlinear rays is to move a coordinate frame along the curve $\mathbf{c}(v)$. We again use the rotation-minimizing coordinate frame of Klok [8]. For each position on the path, a constant number of rays is traced. The initial point of each ray is placed in the plane orthogonal to the path. Note that the gradient is not defined along the path $\mathbf{c}(v)$ since it is a valley line of the distance map $dist(\mathbf{p})$. Therefore, the initial points are placed circularly at a small distance from the path position. Once the initial points have been determined (u parameterization), the rays are traced integrating the negative gradient of the distance map.

The rays have the tendency to be perpendicular to the path $\mathbf{c}(v)$. This is the direction of maximal change of $dist(\mathbf{p})$ in linear segments of the path. The rays become curved in areas where the curvature of the path increases.

Colon Surface Parameterization

In the previous section, nonlinear and non-crossing rays were traced from the central path $\mathbf{c}(v)$ towards the colon surface. While the rays are traced, direct volume rendering is performed. The ray terminates when the colon surface is hit. The result of the nonlinear ray casting is a sampling of the inner surface of the organ.

The tracing of the nonlinear rays defines an unambiguous parameterization of the inner colon surface $\mathbf{s}(u, v)$. Here, v is the parameter along the central path $\mathbf{c}(v)$, and u is the radial angle along which the nonlinear rays are started ($u \in [0, 2\pi]$).

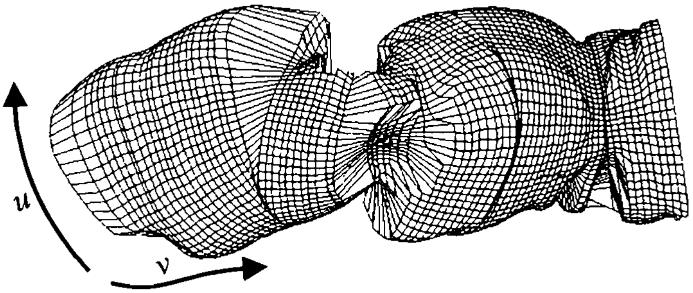

Fig. 6. Surface obtained after nonlinear ray casting. The sampling of the surface is nonuniform.

Figure 6 shows $\mathbf{s}(u, v)$ which results from applying nonlinear ray casting to a colon piece. The lines correspond to the isolines of the parametric surface $\mathbf{s}(u, v)$. The parameter space is sampled uniformly in the u and v direction, but this does not correspond to a uniform sampling of $\mathbf{s}(u, v)$.

Unfolding of the $\mathbf{s}(u, v)$ surface can easily be done by mapping $\mathbf{s}(u, v)$ onto a regular grid in the 2D u, v-parameter space. In figure 7a, parameterization of the colon surface is done with straight rays (ambiguous parameterization and non-uniform sampling). In figure 7b, a parameterization of the colon surface is done with curved rays (unambiguous parameterization, but still non-uniform sampling).

Nonlinear ray casting avoids that features appear more than once, but on the other hand the sampling of the surface is far from being uniform. There are over-sampled areas, which lead to geometric deformations, and also undersampled areas exist. In the latter case, deformations appear but also features of the surface can be missed.

In figure 7a, the solid circles indicate areas where features appear more than once. Using nonlinear ray casting, the polyps do not appear more than once, and instead an enlargement of the feature appears (figure 7b). The areas marked by dashed circles indicate undersampled areas and therefore areas where features are possibly missed. Note that the same undersampled areas are present in both figures.

In the next section, an algorithm is presented to obtain an unfolding of the parametric surface $\mathbf{s}(u, v)$ which avoids geometric deformations and undersampling.

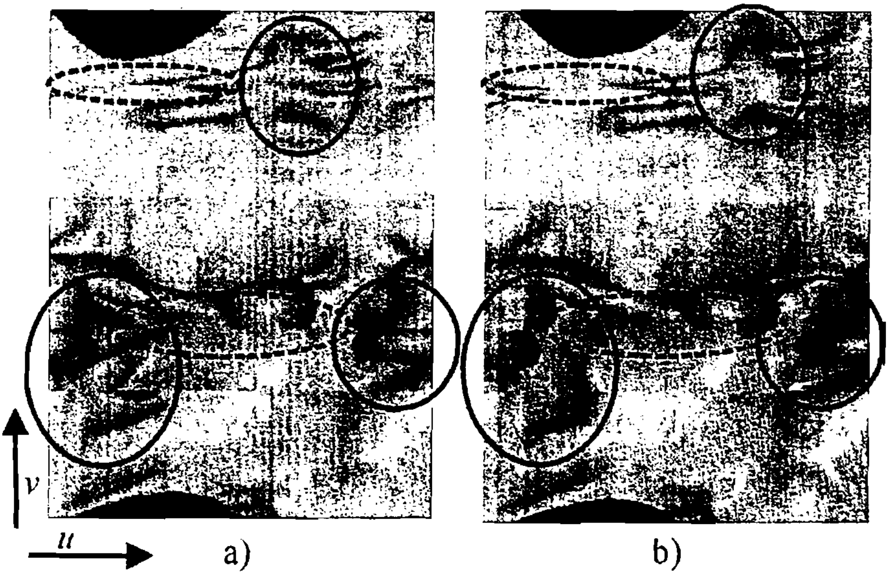

Fig. 7. a) Unfolding of the colon surface of the data set presented in figure 6 using straight rays. Solid circles indicate areas where polyps appear more than once. Dashed circles indicate undersampled areas. b) Parametric surface generated using nonlinear rays as shown in figure 6. Unfolding is done onto a regular grid. Multiple appearance of polyps disappear, but undersampled areas not.

4.2 Nonlinear 2D Scaling

In the previous section, an unambiguous parameterization of the inner colon surface projected to the central path has been introduced. The sampling of the surface $\mathbf{s}(u,v)$ defines a valid and non self-intersecting quadrilateral mesh on the colon surface (see figure 6). Furthermore, the distance between the surface point $\mathbf{s}(u,v)$ and the corresponding path position $\mathbf{c}(v)$ defines a height field $r(u,v)$.

The goal of nonlinear 2D scaling is to achieve a 2D grid (i.e., parameter space) which approximates a parallel projection of the unfolded height field (see 4.1). The unfolded height field shall approximately preserve the length of the edges of $\mathbf{s}(u,v)$ in u- and v-direction.

Height-field Unfolding

In the nonlinear ray casting, a 3D quadrilateral mesh is obtained. We know the distances b_i between adjacent quadrilateral vertices (i.e., the length of the edges of the quadrilateral). If we preserve these distances in the 2D grid (i.e., parameter space), the sizes of the quadrilaterals will be preserved (see figure 8b). However, by preserving the 3D edges of the quadrilateral mesh, we flatten the surface and the polyps. This is due to the fact that we do not take the height field $r(u,v)$ into account. We want that the edges of the 3D quadrilateral mesh are preserved in the unfolded height field. This implies that the distance e between edges in the 2D grid should correspond to the length of the projection of the edges onto the grid plane (see figure 8c).

Using these observations, we define e such that the unfolded height field preserves the length of the edges of the 3D quadrilateral mesh in u and v direction (see Vilanova et al. [16] for details). In the next section, an algorithm to obtain such a 2D grid is presented.

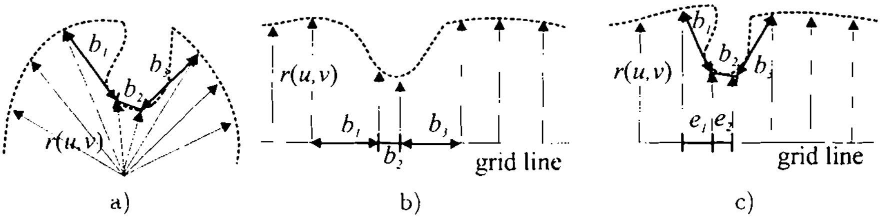

Fig. 8. Illustration of height field unfolding in u direction: a) cross-section of $r(u,v)$ for a fixed value of v, b) unfolding preserving the edge lengths b_i of the 3D quadrilateral mesh in the 2D grid, and c) unfolding preserving the edge lengths b_i of the 3D quadrilateral mesh in the height field.

Nonlinear 2D Scaling

The objective of the nonlinear 2D scaling algorithm is to generate a 2D grid whose edges preserve the length $e(i,j,k,l)$, calculated as explained in the previous section. In $e(i,j,k,l)$, i and k correspond to the ith and kth sampled parameter value in u-direction, and respectively j and l correspond to the jth and kth sampled parameter value in v-direction. Finding an analytical solution to this problem is too complex, so a numerical solution is adopted. We use an approach similar to the one presented by Keahey et al [7]. The main difference is that our algorithm not only preserves areas, but also the edge lengths.

We define a function $\mathbf{T}(i,j) : \mathbb{N}^2 \rightarrow \mathbb{R}^2$ as a transformation of a 2D regular grid. $\mathbf{T}(i,j)$ has to be C^0-continuous and it should preserve the order (i.e., no flipping edge or grid node).

We define a 2D scaling field S as a field of scalar values for each edge. Each scalar value indicates the scaling factor that a transformation $\mathbf{T}$ has applied to the edge. The 2D scaling field S for an edge defined between $\mathbf{T}(i,j)$ and $\mathbf{T}(k,l)$ is $S(i,j,k,l) := \|\mathbf{T}(i,j) - \mathbf{T}(k,l)\|$. A 2D scaling field S is defined for any transformation $\mathbf{T}$.

The goal of the nonlinear 2D scaling algorithm is to find a transformation $\mathbf{T_g}$ such that the equation $e(i,j,k,l) = \|\mathbf{T_g}(i,j) - \mathbf{T_g}(k,l)\|$ holds for all values of (i,j), where (k,l) is a 4-connected neighbor of (i,j). In other words, we want to find a transformation $\mathbf{T_g}$ whose 2D scaling field is $S_g(i,j,k,l) = e(i,j,k,l)$ for each edge of the grid.

The major problem is to find the coordinates (x,y) of the transformation $\mathbf{T_g}$, given the scalar values of the 2D scaling field S_g. It is clear that for the same 2D scaling field several transformations are possible. We have used an iterative method which provides a numerical solution. The goal of the algorithm is to find a transformation $\mathbf{T_a}$ that provides a good approximation of $\mathbf{T_g}$.

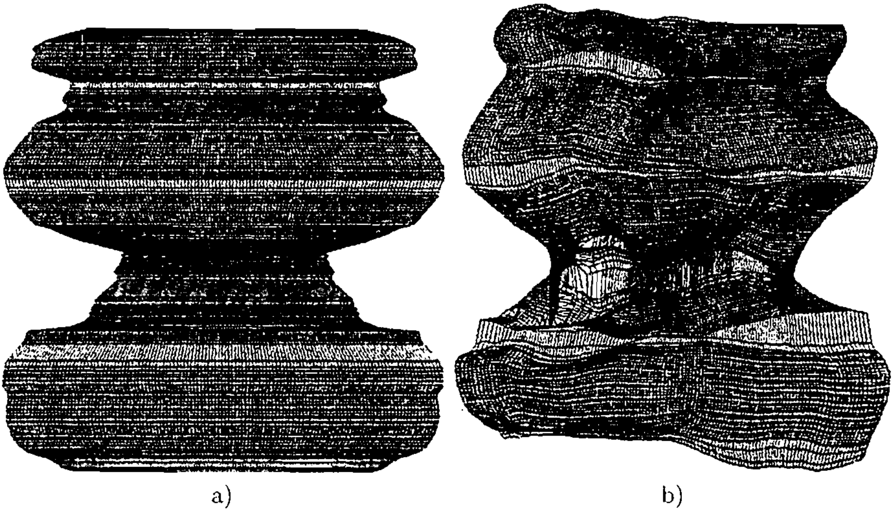

Fig. 9. Illustration of the nonlinear 2D scaling algorithm using the same data set as in figure 6. a) Initial $\mathbf{T_a}$ corresponding to a 128x171 grid. b) $\mathbf{T_a}$ after 960 iterations of the algorithm.

Given a transformation $\mathbf{T_a}$, the corresponding scaling field S_a can easily be calculated. A scaling field error can then be computed by $S_e = S_g - S_a$. S_e gives the difference between the current scaling field S_a and the desired scaling field S_g.

The iterative algorithm starts with T_a as a regular grid. Then S_a and S_e are calculated. The algorithm iterates over each node of the grid. For each node, the value of S_e at each of the 4-connected neighbors is investigated. If $S_e > 0$ (i.e., the edge is not long enough) then the neighbor is moved away from the node . If $S_e < 0$ (i.e., the edge is too long) then the neighbor is pulled towards the node. The edge is modified by a length of $S_e(i,j,k,l)C_r/2$ where $C_r \in [0,1]$ is a parameter of the algorithm. The division by 2 is necessary because each edge is treated twice, once for each vertex of the edge. Changing an edge is thus done by modifying each of its vertices. An important requirement of the algorithm is to preserve the order. So the neighbors are moved as far as S_e and C_r allow without flipping edges.

The neighboring nodes are changed with coordinate-aligned movements. These movements have the tendency to preserve the rectangular appearance defined by $\{\mathbf{T_a}\ (i,j), \mathbf{T_a}\ (i+1,j), \mathbf{T_a}\ (i+1,j+1), \mathbf{T_a}\ (i,j+1)\}$, which, for example, does not degenerate to a triangle.

Once the iteration has run for all the nodes, the new $\mathbf{T_a}$ is generated. Then, a new S_a and a new S_e are calculated from the resulting $\mathbf{T_a}$. S_e is calculated just once per iteration.

The convergence factor is measured using the distance between the approximating scaling field S_a and the desired 2D scaling field S_g. This is expressed as the root mean squared error σ of S_e.

The convergence of the algorithm can be improved by starting with a $\mathbf{T_a}$ which is a closer approximation of the desired result than a regular grid. The length of the edges within a horizontal line (i.e., the horizontal edges between nodes with the same j value) are set such that the line length approximates the perimeter of the colon in the corresponding cross-section. The distance between two consecutive horizontal lines is set to the average of the vertical edge lengths in S_g which join the nodes between the two lines (see figure 9a). This initial modified grid leads to a faster convergence by generating basically the same result as a regular grid would give.

The complexity of the nonlinear 2D scaling algorithm is $O(k \cdot n \cdot m)$ where $n \times m$ is the size of the original grid and k is the number of iterations needed for convergence.

Figure 9a shows the initial grid $\mathbf{T_a}$ for the segment of the colon presented in figure 6. The resolution of the grid is 128x171 and the initial value of σ is 0.8008. After 960 iterations $\mathbf{T_a}$ has been evolved into the grid in figure 9b. The value of σ is 0.2808.

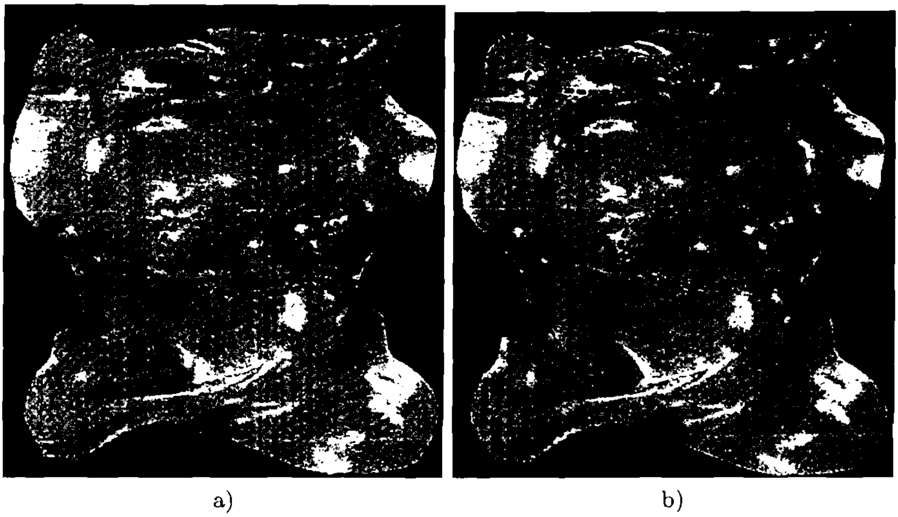

Fig. 10. Resampling after the nonlinear 2D scaling. a) 128x171 shaded grid using bilinear interpolation. b) Shading of the resampled grid.

4.3 Resampling

The nonlinear 2D scaling provides a mapping between the 3D quadrilateral mesh and a 2D grid avoiding area deformations. The color of each ray obtained in the nonlinear ray casting step is assigned to its corresponding node in the 2D grid. Bilinear interpolation is used to fill the quadrilaterals of the grid. An example can be seen in figure 10a. The areas encircled by dashed ellipses are the same as in figure 7. Some features are missing due to undersampling.

The undersampled areas are easily identifiable from the 2D grid. A minimum sample step for the 2D grid is defined. The sample step corresponds directly to a sample step in the 3D space. For each quadrilateral, the subdivision consists of generating a subgrid whose edge lengths are smaller than or equal to the sample step.

Each of the newly generated nodes in the grid can easily be identified with its corresponding point in 3D using linear interpolation. The 3D points do not correspond to surface points, but they are close to the colon surface. A short nonlinear ray segment through the point is investigated to locate the correct surface point. Then the rays are traced forward again to find the correct surface point.

The resulting color values are mapped directly to the corresponding point in the 2D grid. The results of the resampling procedure can be seen in figure 10b. The encircled areas show regions where features that were not present in figure 10a have been identified.

4.4 Results

The CT volume data of an extracted colon with a resolution of 381x120x632 is used in our experiments (see figure C.33 right top). The colon is 50 cm long and contains 13 polyps. The unfolding of this colon can be seen in figure C.33 to the left. All the polyps could be detected easily by inspection. The extracted colon was physically dissected and several pictures of the dissected colon were also taken. These pictures enable a qualitative comparison between the real data and the results of the presented algorithm (see figure C.33).

5 Conclusions

Simulating an endoscopic view is not the most suitable visualization technique in many endoscopy procedures. For example, if the physician is interested in inspecting the inner surface of the organ, the endoscopic view visualizes just a very small percentage of it. This chapter presented various techniques which generated an unfolded model of a colon. This unfolded model allows a more efficient visualization of the inner surface. They are generated by projection, resampling and/or adequate parameterization of the organ.

Section 3 describes a technique that locally unfolds the colon, and generates an animation sequence from consecutive unfolded regions. The images allow the physician to visualize most of the surface, and to easily recognize polyps that would be hidden in an endoscopic view by folds or would be hard to localize. For more examples refer to `www.cg.tuwien.ac.at/research/vis/vismed/ColonFlattening/`.

With the previous method, the physician has to inspect a video to be able to visualize the whole surface. The colon-unfolding technique in section 4 enables the physicians to get a fast overview of the entire organ surface within a single image. This approach solves the problem that previous techniques had [20]. Compensation of area distortions due to the unfolding is achieved using an iterative method. However angle distortions are not taken into account. For more results refer to `www.cg.tuwien.ac.at/research/vis/vismed/ColonUnfolding/`.

The methods presented in chapters 3 and 4 have been tested with a data set that enabled a qualitative comparison of the resulting images with images of the corresponding real extracted colon with satisfactory results.

These techniques present a new way to parameterize the organs in order to inspect their inner surface.

Acknowledgements

The work presented in this publication has been funded by the Adapt project. Adapt is supported by *Tiani Medgraph*, Vienna, and the *Forschungsförderungsfonds für die gewerbliche Wirtschaft*, Austria. We thank Dr. Erich Sorantin from the Department of Radiology in Graz for his collaboration and for providing the data sets and the images of the dissected colon.

References

1. R. H. Abraham and C. D. Shaw. *Dynamics: The Geometry of Behavior.* Addison-Wesley, 1992.
2. C. Bennis, J.M. Vézien, and G. Iglésias. Piecewise surface flattening for non-distorted texture mapping. In *SIGGRAPH'91, Conference Proceedings*, pages 237–246, 1991.
3. M.S. Floater. Parametrization and smooth approximation of surface triangulation. *Computer Aided Geometric Design*, 14:231–250, 1997.
4. E. Gröller. Nonlinear ray tracing: Visualizing strange worlds. *The Visual Computer*, 11:263–274, 1995.
5. S. Haker, S. Angenent, A. Tannenbaum, and R. Kikinis. Nondistorting flattening maps and the 3D visualization of colon CT images. *IEEE Transactions on Medical Imaging*, 19(7):665–671, July 2000.
6. S. Haker, S. Angenent, A. Tannenbaum, R. Kikinis, G. Sapiro, and M. Halle. Conformal surface parameterization for texture mapping. *IEEE Transactions on Visualization and Computer Graphics*, 6(2):181–189, April-June 2000.
7. T.A. Keahey and E.L. Robertson. Techniques for non-linear magnification fields. In *IEEE Information Visualization'97, Conference Proceedings*, pages 51–58, 1997.
8. F. Klok. Two moving coordinate frames for sweeping along a 3D trajectory. *Computer Aided Geometry Design*, 3:217–229, 1986.
9. B. Lévy and J.L. Mallet. Non-distorted texture mapping for sheared triangulated meshes. In *SIGGRAPH'98, Conference Proceedings*, pages 343 352, 1998.
10. G. Lohmann. *Volumetric Image Analysis.* Chichester Wiley, 1998.
11. B. O'Neill. *Elementary Differential Geometry.* Academic Press, 1966.
12. D.S. Paik, C.F. Beaulieu, R. B. Jeffrey, Jr. C.A. Karadi, and S. Napel. Visualization modes for CT colonography using cylindrical and planar map projections. *Journal of Computer Tomography*, 24(2):179–188, 2000.
13. M. Samek, C. Slean, and H. Weghorst. Texture mapping and distortion in digital graphics. *The Visual Computer*, 2:313–320, 1986.
14. I.W.O. Serlie, F.M. Vos, R.E. Van Gelder, J. Stoker, R. Truyen, Y. Nio, and F.H. Post. Improved visualization in virtual colonoscopy using image-based rendering. In *VisSym '01 Joint Eurographics - IEEE TCVG Symposium on Visualization, Conference Proceedings*, pages 137–146. Springer, 2001.

15. A. Vilanova Bartrolí, A. König, and E. Gröller. Cylindrical approximation of tubular organs for virtual endoscopy. In *Computer Graphics and Imaging 2000, Conference Proceedings*, pages 283–289. IASTED/ACTA Press, November 2000.
16. A. Vilanova Bartrolí, R. Wegenkittl, A. König, and E. Gröller. Nonlinear virtual colon unfolding. In *IEEE Visualization 2001, Conference Proceedings*, pages 411–418, October 2001.
17. A. Vilanova Bartrolí, R. Wegenkittl, A. König, E. Gröller, and E. Sorantin. Virtual colon flattening. In *VisSym '01 Joint Eurographics - IEEE TCVG Symposium on Visualization, Conference Proceedings*, pages 127–136, May 2001.
18. G. Wang, S.B. Dave, B.P. Brown, Z. Zhang, E.G. McFarland, J.W. Haller, and M.W. Vannier. Colon unraveling based on electrical field: Recent progress and further work. In *SPIE, Conference Proceedings*, volume 3660, pages 125–132, May 1999.
19. G. Wang, E. G. McFarland, B. P. Brown, and M. W. Vannier. GI tract unraveling with curved cross sections. *IEEE Transactions on Medical Imaging*, 17:318–322, 1998.
20. G. Wang and M.W. Vannier. GI tract unraveling by spiral CT. In *SPIE, Conference Proceedings*, volume 2434, pages 307–315, 1995.
21. R. Wegenkittl, A. Vilanova Bartrolí, B. Hegedüs, D. Wagner, M. C. Freund, and E. Gröller. Mastering interactive virtual bronchioscopy on a low-end PC. In *IEEE Visualization 2000, Conference Proceedings*, pages 461–464, October 2000.